Self-organized three-band structure of the doped fermionic Ising spin glass

H. Feldmann[1] and R. Oppermann[1,2]
[1]*Institut für Theoretische Physik, Universität Würzburg, D-97074 Würzburg, Federal Republic of Germany*
[2]*Department of Physics, University of Oxford, 1 Keble Road, Oxford OX1 3NP, United Kingdom*
(Received 5 October 1999; revised manuscript received 22 February 2000)

The fermionic Ising spin glass is analyzed for arbitrary filling and for all temperatures. A self-organized three-band structure of the model is obtained in the magnetically ordered phase. Deviation from half-filling generates a central nonmagnetic band, which becomes sharply separated at $T=0$ by (pseudo)gaps from upper and lower magnetic bands. Replica symmetry breaking effects are derived for several observables and correlations. They determine the shape of the three-band density of states, and, for given chemical potential, influence the fermion filling strongly in the low-temperature regime.

I. INTRODUCTION

Frustrated magnetic correlations in fermionic systems are the subject of current and promising research in modern condensed-matter theory. Generalized (fermionic) spin glass models and certain Hubbard models form two model classes for theoretical investigations of these phenomena in disordered and clean systems, respectively. The coupling to a particle reservoir allows to control important parameters such as fermion concentration or effective spin density by means of a chemical potential. The important experimental tool of doping often leads to quantum phase transitions (QPT), metal-insulator transitions, or magnetic phase transitions being prominent and standard examples thereof. The chemical potential μ (or, alternatively, the fermion filling ν) is thus a relevant variable for the phase diagram. In quantum spin glass theory, a well-known model showing a QPT as the effect of a disordering transverse field $h_\perp$ is the transverse field Ising model; in the present paper, the chemical potential μ is considered instead, playing the role of a generalized transverse field: μ couples to the charge, while $h_\perp$ couples to transverse spin degrees of freedom. Since particle number operators and Ising spin operators commute, the chemical potential does not generate quantum spin dynamics. On the other hand, single fermion operators do not commute with the spin interaction and hence quantum dynamics always exists in the fermionic spin glass models. This kind of dynamical behavior is reflected for example in the fermion propagator and its spectral density determines the band structure.

A famous example for doping effects on magnetism is the breakdown of antiferromagnetic order in Hubbard-type models.[1] The doped fermionic Ising spin glass contains a couple of close relationships with the Hubbard model. Comparable phenomena in the band structures appear and will be discussed. However, it must also be noted that problems of perturbative expansions of the Hubbard model leave very controversial the theory of doping effects[2] in contrast to the present case of an insulating fermionic spin glass. A highly interesting comparison of central bands emerging in the (infinite-dimensional) Hubbard model and in Kondo lattices, including a discussion of implications for transport in general and the Mott transition in particular, was given by Nozières.[3]

A. Aim of the paper

It has been the purpose of the present work to explore in detail the dependence on the chemical potential μ, and to improve thus the understanding of the low-temperature glassy phase. The effects of particle hole symmetry breaking and of replica symmetry breaking (RSB) on the band structure are derived for all temperatures and chemical potentials within the ordered phase. It is found that breaking these symmetries splits up a spin glass pseudogap into two similar pseudogaps, which delimit a central nonmagnetic band, the upper gap accommodating the Fermi level. Strong reactions to doping such as crossover and possible new transitions deep in the ordered phase, still far below the critical doping which destroys random magnetic order in favor of the paramagnetic phase, are also reported in this paper. Usually, magnetically interacting systems realize saturated magnetic order in the ground state at zero temperature, even if the interaction is frustrated and random such that magnetic order consists of randomly oriented frozen-in magnetic moments. But doping must be expected to reduce the magnetic order at all temperatures as an effect of the diminished effective spin density. It is well known that spin glass order requires a mean-field theory with more than one order parameter, $q_1, q_2, \ldots, q_{k+1}$ in case of k RSB steps, which, for $k\to\infty$, form the Parisi order-parameter function[4–7] $q(x)$ defined on an interval $0\leqslant x\leqslant 1$. It is a very important question to see how the breakdown of frozen magnetic order at critical doping is approached in the presence of such a relatively complicated order parameter. For this purpose it is the necessary to achieve a full description of the ordered phase including in particular the $T=0$ limit. This is done in the present paper. The results of the paper also show that not only the simple box-shaped form of $q(x)$ at $T=0$, with a box height that equals the saturated Edwards-Anderson order parameter, but also the low-temperature behavior of the order parameter, which was intensively studied once for the standard SK model,[6] plays a role for the band structure of the doped fermionic Ising spin glass.

B. Relations to preceding publications

In previous papers, the density of states of the fermionic Ising spin glass (ISG_f) was analyzed in detail for half filling.[8] A pseudogap was obtained in a solution with infi-

nitely many steps of replica symmetry breaking (RSB). Hence the effect of this infinite breaking of the discrete symmetry resembled the one of breaking a continuous symmetry, which commonly leads to soft modes. In the present case, soft single particle excitation energies were created, unrelated to the existence of two-particle soft modes, for which the single particle density of states (DOS) appears only as a weight.

Replica symmetry breaking introduces a sort of statistical fluctuation effects in fermionic spin glasses, which determine the band shape. In particular the softening of gap energies occurs like a one-dimensional quantum critical phenomenon.

This single dimension can be viewed as the replica dimension, while a similar role is played by the time in the dynamic mean-field theory of the infinite-dimensional Hubbard model. It was, however, also found for the ISG_f that the finer structures induced by symmetry breaking in replica space were directly felt in the quantum dynamic behavior of the subclass of fermionic correlations.

The extension to doping and of general arbitrary filling, which affects size, position, and splitting of gaps as described by the results of this paper, has been a nontrivial task. First, the numerical calculations for arbitrary temperatures are rather involved. Moreover, in contrast to half filling, the analytical low-temperature expansion required a different technique which consists in a combination of the saddle-point technique with a generalized Sommerfeld expansion as introduced by da Costa *et al.*[9] The Sommerfeld–da Costa method is built on a low-temperature (formal) analogy between a Fermi distribution and an effective-field distribution in spin glasses: the role of energies close to the Fermi level is in the present case played by the modulus of the effective spin glass field being close to $\mu-\overline{\chi}/2$. This quantity, where $\overline{\chi}$ stands for the Thouless-Anderson-Palmer (TAP) susceptibility,[10] is negative or zero (hence ineffective at $T=0$) for half filling and positive in the doped case. The transition through $\mu=\overline{\chi}/2$ is continuous.

The results of this paper are finally obtained by combined (rather than purely complementary) numerical and analytical analysis. This ''numerico-analytical'' study is based on a replicated field-theoretical treatment of the random Ising interaction problem.

The present paper also involves and revisits earlier results for the tricritical phase diagram[11] away from half filling.

The low-temperature limit of the non-half-filled model and the way the phase transition into the paramagnetic phase takes place had still been an open problem. This was related to several problems: first, information about the full replica-broken solution [removing a negative Almeida-Thouless (AT) eigenvalue] was only available at half filling, and secondly, another AT eigenvalue turns complex due to the replica limit and the question of stability is raised again. In this article we assume that the solution according to standard replica symmetry breaking is stable throughout the ordered phase (see a more detailed discussion of the stability properties in Refs. 12 and 13).

C. Outline of the paper and a guide to the reader

Section II is devoted to a concise presentation of the model and of some of the formalism used here. The main part of the paper, Sec. III, presents numerical (for all temperatures) and analytical results (at $T=0$) for the fermionic density of states. Intermediate results for order parameters, fermion concentration, and relevant susceptibilities, interesting in its own right, are in contrast to the dynamical propagator determined from the free energy. In the first part of Sec. III the replica symmetric approximation is solved, the three-band structure being already revealed, yet with a crude approximation of gaps. The second part presents one-step symmetry broken solutions, which provide in comparison with the zeroth approximation a good outlook on the exact solution. The extension to infinite breaking and of its key features is discussed and can be visualized rather easily by comparing, e.g., Fig. 2 with Fig. 7, and also Fig. 4 with Fig. 8. The splitting of the spin glass generated charge gap under particle-hole symmetry breaking (finite μ) and the related central nonmagnetic band are the important results, which must have implications on the behavior of weakly itinerant generalized models (to be studied in the future).

The reader, who is interested primarily in the currently most advanced *analytical* results (in 1RSB approximation) may jump to Eq. (28), using the definitions (6) and (23) together with the free energy of Eq. (22), which is sufficient to determine self-consistently and uniquely all parameters needed in Eq. (28). Intermediate results are also given. A first experience with the numerical and analytical nonperturbative technical difficulties may, however, be sought at the level of replica symmetric equations given in Sec. III A up to Eq. (21).

In Sec. IV the spin glass effect on the averaged fermion concentration is shown: magnetic order introduces rather strong replica symmetry breaking effects into this simplest charge related quantity. The one-step symmetry broken approximation shows a kind of transition inside the ordered phase, as can be seen in Figs. 9 and 10 (left). Moreover, a nice agreement is found with an independent numerical solution of the corresponding TAP problem for $\nu(\mu)$. The result shows how RSB effects, caused by the frustrated spin interactions alone, are also felt in charge variables because of the coupled charge and spin fluctuations.

II. DOPED FERMIONIC ISING SPIN GLASS

The ISG_f and some of its extensions have been discussed in preceding publications.[12,14,15] For this reason we only include in this introductory section an overview over those features of the model and of the technicalities that are necessary to understand the present work.

The grand canonical Hamilton operator

$$\mathcal{K}=-\sum_{i<j} J_{ij}\sigma_i^z\sigma_j^z-\mu\sum_i n_i \tag{1}$$

introduces the many-body interaction of fermionic spins with fully frustrated random couplings J_{ij}. Stripping off the factor $\hbar/2$, the spin and occupation number operators σ^z and n are given by the fermion operators as $\sigma^z=a_\uparrow^\dagger a_\uparrow-a_\downarrow^\dagger a_\downarrow$ and $n=a_\uparrow^\dagger a_\uparrow+a_\downarrow^\dagger a_\downarrow$, respectively. We choose the random interaction couplings to be distributed by

$$\mathcal{P}(J_{ij})=\frac{1}{\sqrt{2\pi}J}e^{-J_{ij}^2/(2J^2)}. \tag{2}$$

This generates magnetic correlations independent of time and of infinite range in real space. For the sake of clarity we will below keep the variance J^2 as a parameter in the formulas, whereas it is set equal to unity in the numerical evaluations.

Particle-hole transformation and the $\mu \leftrightarrow -\mu$ symmetry. The Hamiltonian (1) is invariant under the particle-hole transformation $a \leftrightarrow a^\dagger$ only at $\mu=0$, but up to a constant it is invariant under $(a \leftrightarrow a^\dagger, \mu \leftrightarrow -\mu)$ for all μ. Thus we can restrict the discussion of the density of states to the case of non-negative chemical potential, which implies a filling factor $\nu \geqslant 1$. Results for hole doping can be obtained by substituting μ by $-\mu$ and ν by $2-\nu$.

The average over the interaction distribution is performed by means of the replica trick. The averaged replicated partition function can be obtained in terms of Grassmann fields ψ, $\overline{\psi}$, being the usual anticommuting eigenvalues of the original fermion operators a and $a^\dagger$ in the fermionic coherent states. Including also generating (anticommuting) fields $\eta, \overline{\eta}$, the partition function in these fields (generating functional) is given by

$$\langle Z^n \rangle_{\rm av} = \int \{\mathcal{D}J_{ij}\} \int \{\mathcal{D}\overline{\psi}^{a\tau}_{i\sigma} \mathcal{D}\psi^{a\tau}_{i\sigma}\} \left(\prod \mathcal{P}(J_{ij}) \right) \times \exp \int_0^{1/T} d\tau \left(-\overline{\psi}^{a\tau}_{i\sigma} \partial_\tau \psi^{a\tau}_{i\sigma} - \mathcal{K} + \eta^{a\tau}_{i\sigma} \overline{\psi}^{a\tau}_{i\sigma} - \overline{\eta}^{a\tau}_{i\sigma} \psi^{a\tau}_{i\sigma} \right). \tag{3}$$

In the grand canonical Hamiltonian $\mathcal{K}$ the Grassmann fields ψ and $\overline{\psi}$ also replaced the original fermion operators. In the exponent of Eq. (3) the summation convention over replica index a, spin index σ, and site index i is assumed. The subsequent steps, which are described in detail in Refs. 14 and 15, are listed by: explicit Gaussian integration over the J_{ij}, transformation from imaginary times τ to fermionic Matsubara frequencies $\epsilon_l = (2l+\frac{1}{2})\pi T$, and two consecutive decoupling procedures. An eight-fermion correlation term is broken down by a matrix field Q. The saddle-point solution $\langle Q^{ab} \rangle$ is chosen in accordance with Parisi's replica symmetry breaking (RSB) scheme, before a second decoupling to bilinear Grassmann terms can be achieved using auxiliary (c-number) decoupling fields z_i. The $\langle Q \rangle$ matrix stands for the spin correlations $\langle \sigma^a \sigma^b \rangle$, introducing the off- diagonal (replica-overlap) order parameters $q_1, q_2 \cdots q_{k+1}$ according to the Parisi scheme[4,5] and the diagonal one $\tilde{q} \equiv \langle Q^{aa} \rangle$ which takes care of the spin autocorrelation function for $a=b$.

After all, the replicated partition function is expressed as

$$\langle Z^n \rangle_{\rm av} = \exp\left(-\frac{J^2}{4T^2} \mathrm{Tr}\, Q^2 \right) \int \{\mathcal{D}\overline{\psi}^{al}_\sigma \mathcal{D}\psi^{al}_\sigma\} \times \left\{ \prod_k \int_{z_k}^{G} \right\} \exp\left(\overline{\psi}^{al}_\sigma g^{-1}_{al\sigma} \psi^{al}_\sigma + \eta^{al}_\sigma \overline{\psi}^{al}_\sigma - \overline{\eta}^{al}_\sigma \psi^{al}_\sigma \right), \tag{4}$$

where the site index has disappeared due to the infinite-range assumption and the resulting space-homogeneous saddle point. The abbreviations

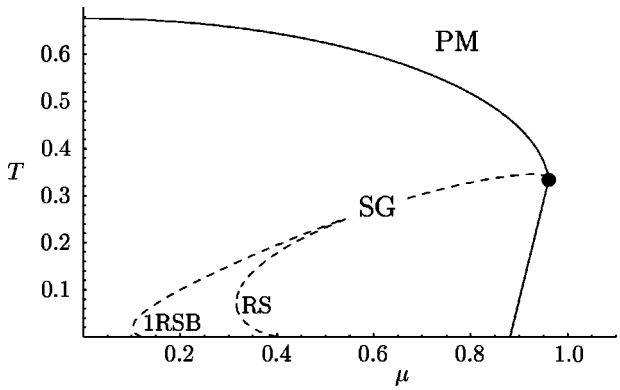

FIG. 1. Phase diagram of the ISG_f (T and μ displayed in units of J). The straight line connecting the tricritical point at ($\mu = 0.961J$, $T = J/3$) with the $T=0$ first order transition at $\mu = 0.881J$ approximates linearly the thermodynamic first-order transition into the paramagnetic phase (PM). The dashed lines locate the crossover line $\partial^2 f / \partial \tilde{q}^2 = 0$ connected to the appearance of a central density-of-states peak in replica symmetric (RS) and in one-step symmetry broken (1RSB) approximation, respectively. At ∞RSB this line will reach the point ($T=0, \mu=0$).

$$g^{-1}_{al\uparrow} = \tilde{H}^a + i\epsilon_l + \mu,$$
$$g^{-1}_{al\downarrow} = -\tilde{H}^a + i\epsilon_l + \mu, \tag{5}$$
$$\tilde{H}^a = J\sqrt{q_k} z_{k+1} + J\sqrt{q_{k-1} - q_k} z_k + \cdots + J\sqrt{\tilde{q} - q_0} z_0^a$$

illustrate the evolution of a fermion, described by the nonaveraged inverse propagator g^{-1}, in a realization of the random effective field $\tilde{H}^a$ [spatial propagation is excluded by the definition of model (1)]. The Gaussian integrals, which appear frequently throughout the paper and which describe the probability of the realizations of the effective field $\tilde{H}$, has been reduced to the short form

$$\int_z^G \phi(z) \equiv \frac{1}{\sqrt{2\pi}} \int_{-\infty}^{\infty} dz e^{-(1/2)z^2} \phi(z). \tag{6}$$

After this field-theoretical setup the free energy and the generating functional, respectively, are obtained by means of the replica trick, $f = \lim_{n\to 0} (T/n)(1 - \langle Z^n \rangle|_{\eta=0})$. For fermionic correlation functions the derivatives with respect to the η fields are taken prior to the $n \to 0$ limit, e.g., for the Green's function

$$G^{aa}_\sigma(i\epsilon_l) = \lim_{n\to 0} \frac{1}{\langle Z^n \rangle_{\rm av}} \frac{\delta}{\delta \eta^{al}_\sigma} \frac{\delta}{\delta \overline{\eta}^{al}_\sigma} \langle Z^n \rangle_{\rm av}. \tag{7}$$

Using standard criteria of thermodynamics, one obtains the phase diagram of the ISG_f as shown in Fig. 1. (We set k_B, and $\hbar$ equal to 1 everywhere in the paper, and display energies in all figures in units of J.)

A tricritical point separates a line of second order transition at high temperatures from first order transitions at low temperatures. The latter phase boundary is very hard to obtain numerically. We therefore approximated it as a straight line down to the best known estimate for the $T=0$ transition, which is obtained below.

III. MAGNETIC AND NONMAGNETIC BANDS

A. Replica symmetric results

Despite its instability against RSB the replica symmetric solution is nontrivial and must be understood in detail, since it forms the basis for the improved solution presented below. Moreover, in a relatively simple description, this approximation contains features of the self-organized transition from single-band structure above freezing temperature to either two bands for half filling or a three-band structure, which occur below freezing of the magnetic moments. The quality of this approximation decreases in the low-temperature regime, as the next section will show. The role of symmetry breaking amounts to a softening of the gaps and to a removal of sharp dropoffs of the density of states at low temperatures, as demonstrated earlier for the case of half filling.[8] At half filling, a pseudogap results between upper and lower magnetic band.

In this section we first present self-consistent numerical solutions for the temperature range from the filling-dependent freezing temperature down to very low T of order $10^{-4}J$. The evaluation of the density of states employs numerical solutions of the self-consistency equations for spin glass order parameter q and linear susceptibility χ as a function of temperature and parametrized by the chemical potential μ. The fermion concentration is also calculated as a function of μ. This analysis is supplemented by an exact $T=0$ calculation.

1. Free energy and resulting self-consistency equations at finite temperatures

The following results are derived from the effective Lagrangian and from a generating functional for general fermionic correlation functions of the model. Analytical solutions are found in the sense that the number of nested integrations becomes minimized before, in a final step, the observables are evaluated numerically. In order to facilitate the zero-temperature limit, it is useful to change variables by introducing the linear susceptibility $\chi=(J/T)(\tilde{q}-q)$. Since $\tilde{q}-q$ decays linearly with T in this limit, the finite linear susceptibility is a helpful quantity which reduces the degree of $1/T$ divergences (which need to be compensated). For this reason f is better expressed in terms of q and χ than in terms of q and $\tilde{q}$.

The free energy (density) f is obtained in the replica symmetric approximation as

$$f=\frac{1}{4}J\chi\left(\frac{\chi T}{J}+2q-2\right)-T\ln 2-\mu-T\int_z^G \ln \mathcal{C} \tag{8}$$

with

$$\mathcal{C}=\cosh\left(\frac{J\sqrt{qz}}{T}\right)+\cosh\left(\frac{\mu}{T}\right)e^{-(1/2T)J\chi}. \tag{9}$$

Extremalization of expression (8) with respect to q, χ, and μ yields the coupled self-consistency equations

$$0=\partial_q f=\partial_\chi f \tag{10}$$

and allows us to determine the filling factor

$$\nu=-\partial_\mu f. \tag{11}$$

The results are finally used in the band-structure calculation.

2. Energy and self-consistency equations in the T=0 limit

The zero temperature limit deserves separate attention for several reasons. As can be seen from the thermal free energy, divergences in this limit trouble the numerical work at low temperatures, but nondivergent analytical results provide a control.

In this case, an analytical approximation was also obtained, applying an expansion in powers of $\mu-\chi/2$. Good agreement was found almost up to the magnetic breakdown.

The equations for $T=0$ were obtained by a variant[9] of the Sommerfeld method. For the density of states the steepest descent method is used in addition. As usual, this limit allows to simplify the equations. We obtain for $\mu<\frac{1}{2}J\chi$

$$E\equiv f(T=0)=\frac{1}{2}J\chi(q-1)-\mu-\sqrt{\frac{2}{\pi}}J\sqrt{q} \tag{12}$$

while for $\mu>\frac{1}{2}J\chi$, the $T=0$ energy becomes

$$E=\frac{1}{2}J\chi(q-1)-\mu-\left(\mu-\frac{1}{2}J\chi\right)\mathrm{erf}\left[\frac{1}{\sqrt{2q}}\left(\frac{\mu}{J}-\frac{\chi}{2}\right)\right]$$
$$-J\sqrt{\frac{2q}{\pi}}e^{-(1/2q)(\mu/J-\chi/2)^2}. \tag{13}$$

Extremalization of these energies yields self-consistency equations which couple the magnetic correlations q and χ with the filling factor as a charge average.

For $\mu/J>\chi/2$ we derive the following relations between zero-temperature parameters:

$$q=1-\mathrm{erf}\left[\frac{1}{\sqrt{2q}}\left(\frac{\mu}{J}-\frac{\chi}{2}\right)\right],\quad \chi=\frac{2}{\sqrt{2\pi q}}e^{-(1/2q)(\mu/J-\chi/2)^2}, \tag{14}$$

$$\nu=1+\mathrm{erf}\left[\frac{1}{\sqrt{2q}}\left(\frac{\mu}{J}-\frac{\chi}{2}\right)\right],\quad q=\tilde{q}=2-\nu. \tag{15}$$

One may derive these solutions as a function of either ν or μ. The $T=0$ relations $q=\tilde{q}$ and $\tilde{q}=2-\nu$ hold also for $0\leq\mu/J<\chi/2$, whereas in this interval one simply obtains

$$\nu=2-\tilde{q}=1,\quad \chi=\frac{2}{\sqrt{2\pi q}}. \tag{16}$$

3. Density of states

The density of states is obtained as usual from the Matsubara Green's function by analytic continuation

$$\rho(\epsilon)=-\frac{1}{\pi}\mathrm{Im}\,G(\epsilon+i0) \tag{17}$$

at any order of RSB. In terms of the shifted variable $E=\epsilon+\mu$ the DOS is symmetric and reads in RS approximation

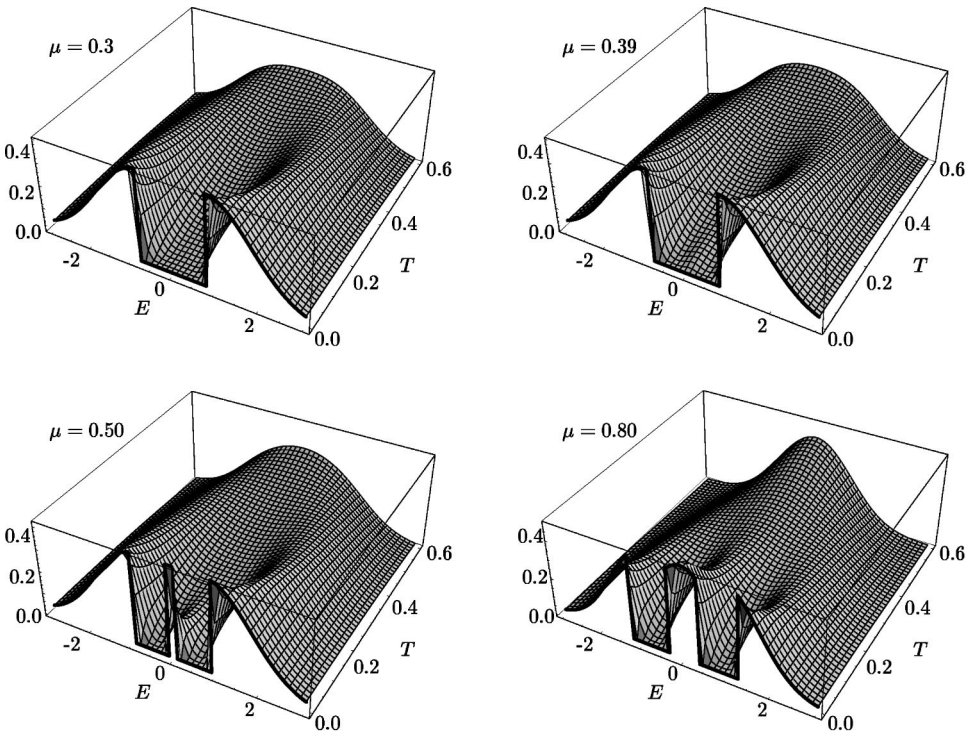

FIG. 2. Density of states $\rho(T,E=\epsilon+\mu)$ shown as a function of all T below the freezing temperature, as calculated in the replica symmetric approximation at specific chemical potentials μ (in units of J). The bold front line represents the independent analytical $T=0$ result.

$$\rho(E)=\frac{\cosh\frac{\mu}{T}+\cosh\frac{E}{T}}{\sqrt{2\pi TJ\chi}}\int_z^G\frac{1}{C}\exp\left(-\frac{(E-J\sqrt{q}z)^2}{2TJ\chi}-\frac{J\chi}{2T}\right). \tag{18}$$

The solutions for $q(\mu,T)$ and $\chi(\mu,T)$ are employed in the calculation of the electronic density of states for the whole spin glass phase. The set of Fig. 2 shows that a central band emerges for high enough chemical potentials. In the RS approximation the band gap discussed previously for half filling[8] is visible up to $\mu=\frac{1}{2}E_g^{(0)}=J/\sqrt{2\pi}$. When the chemical potential approaches the band-gap value (we show for example the DOS at $\mu=0.39J$), a tiny central band shows up at low temperatures, but loses its weight again completely in the $T\to 0$ limit in favor of the magnetic side bands. One can connect this feature to a line given by $\partial^2 f/\partial\tilde{q}^2=0$, which, starting at the tricritical point of the phase diagram, bends into the gap edge[12] at $T=0$. This line, which is also shown in the phase diagram in Fig. 1, wraps this small precursor of the central band (see Fig. 1). For chemical potentials exceeding the gap edge value $J/\sqrt{2\pi}$, the central band emerges already at higher T and survives at $T=0$, where it becomes a pure Gaussian function of $E=\epsilon+\mu$ with finite height and symmetric cutoffs. In the RS approximation both the central band and the magnetic bands are sharply cut off and separated by gaps of identical width χ. As replica symmetry breaking will show, the gap size is given by the nonequilibrium susceptibility $\overline{\chi}$, which agrees with χ only in this lowest order approximation—in this section we continue to discuss the gap in terms of χ. This quantity which separates central from upper band and central from lower magnetic band begins to vary with μ for $\mu>\frac{1}{2}E_g^{(0)}$.

Figure 2 combines the numerical finite temperature calculations of $\rho(T>0,\epsilon)$ with the exactly calculated function $\rho(T=0,\epsilon)$ given below, making use of the numerical solutions for order parameter and susceptibility. As emphasized by the thick lines, the $T=0$ density of states can be decomposed into isolated contributions of the three bands. Taking advantage of the symmetry one may use the energy variable $E\equiv\epsilon+\mu$,

$$\rho(T=0,E)=\rho_-(0,E)+\rho_c(0,E)+\rho_+(0,E), \tag{19}$$

where the central charge band is given by

$$\rho_c(0,E)=\frac{1}{J\sqrt{2\pi q}}e^{-E^2/(2J^2q)}\Theta(\mu/J-\chi/2-|E|/J). \tag{20}$$

Upper and lower magnetic bands contribute

$$\rho_\pm(0,E)=\frac{1}{J\sqrt{2\pi q}}e^{-(|E|/J-\chi)^2/(2q)}\Theta[|E|/J-(\mu/J+\chi/2)]. \tag{21}$$

Let us first discuss the numerical results in the RS approximation. Figure 3 shows the redistribution of spectral weight as T decreases for certain fixed values of the chemical potential:

(i) Within the hard gap regime $0<\mu<J/\sqrt{2\pi}$, where $\nu(T=0)=1$, a pronounced central band is absent; only in a small range of low but finite temperatures a tiny midgap peak is observed. We find that its existence is clearly linked to the characteristic line mentioned above. This line separates the domain of the phase diagram, where the free energy is minimized as a function of $\tilde{q}$, from the one where it is maximized. This latter property is unrelated to the well-known maximization of f by the SG order parameter q; in turn the presence of q is needed to render a solution with $\partial^2 f/\partial\tilde{q}^2<0$ stable. For the present case we find a complex

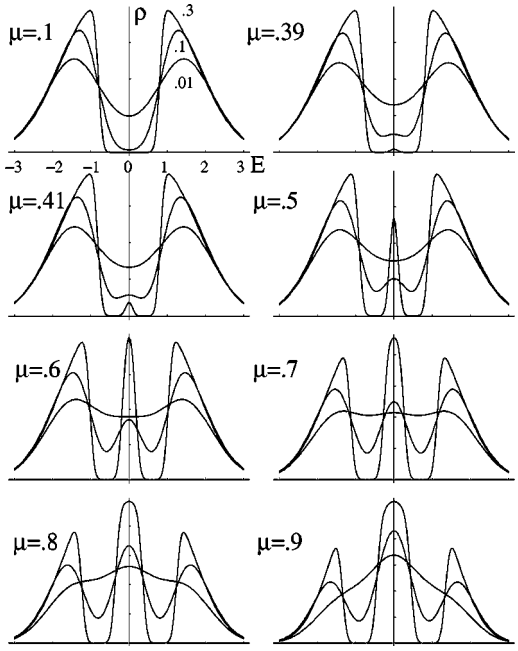

FIG. 3. Density of states: evolution of central peak and thermal band-gap filling for temperatures $T=0.3J,0.1J,0.01J$ at various chemical potentials (displayed in units of J).

Almeida-Thouless eigenvalue (for replica-diagonal perturbation), which does at least not exclude stability apart from the Parisi RSB.

(ii) For chemical potentials large enough to sustain fillings different from one electron per site, i.e., $\mu > J/\sqrt{2\pi}$, three bands develop as the temperature falls below T_f and become separated as $T \to 0$. The Fermi level lies between the central charge band and the upper magnetic band. The area under the central peak belongs to the deviation from half filling, described by $\nu - 1$. The low T results (see Fig. 4) confirm the numerical observation that the central band width is given by $E_{cb}^{(0)} = 2\mu - J\chi$ at $T=0$, that both left and right gap widths obey $E_g^{(0)} = J\chi$, while at half filling the relation reads $E_g^{(0)} = 2J\chi$.

One may compare this approximate solution with an iterated perturbation theory solution of the half filled Hubbard model at zero temperature:[1] there a hopping generated band shows up within the Hubbard gap insulating phase. We do not attempt to discuss any result for itinerant models (in the sense that fermionic hopping terms are allowed in the Hamiltonian), but it is nevertheless clear that the density of states, derived here for the insulating model, can have implications on itinerant systems and their transport behavior. RSB effects, as worked out in the next section, scatter some spectral weight into the hard gap region, exempting the Fermi level. A strong depletion of states remains, however, in the hard gap regions of 0RSB, even for moderate finite temperatures, where RSB effects become negligible. In disordered systems, regions of very small density of states often imply Anderson localized states and in this sense correspond to a hard gap region of a disorder-free model. A metal insulator transition could then occur also as the effect of a dynamical resonance peak (at the Fermi level) generated by a transport mechanism. The present nonitinerant model moreover offers the chance to study how statistical RSB effects shape the central band, and compare this with a dynamical mechanism in disorder-free interaction models.[3] Of course, there are differences between the physical character of these central bands, but it is important to study the similarities too, not only because of the impurity analogy of the $d=\infty$ Hubbard model.[3] A complete comparison will, however, require solutions of the doped Hubbard model and of the itinerant extension of the present spin glass model.

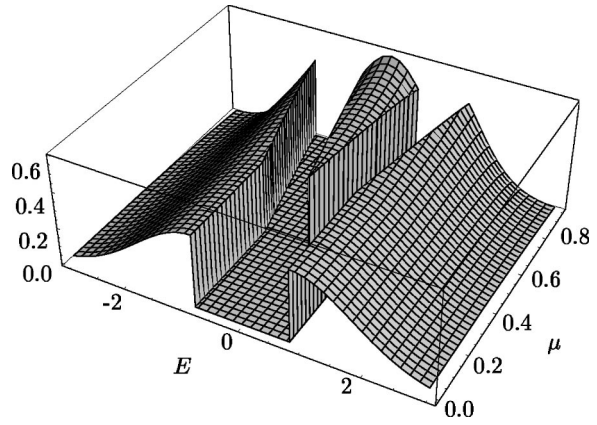

FIG. 4. Density of states as a function of energy E and chemical potential μ at $T=0$ (all quantities shown in units of J). For $\mu > J/\sqrt{2\pi}$ the central charge band appears in the middle of the hard gap at $E=0$. In this case, the Fermi level lies between the central and the upper magnetic band.

We note that the density of states can be used to determine all one particle observables and excitations. For example the fermion concentration, which was given in Eq. (11) as a derivative of the free energy, can be rederived from the Green's function (see Sec. IV below) and may serve as a self-consistency check. It should be remarked that as usual in random systems, the reduction of averaged two particle operators to the averaged one particle Green's function is not possible in general: in particular the Heisenberg equation of motion for a fermion field involves a random interaction in the present case and this must be taken into account in setting up, for example, a relation between thermodynamic potential and one particle Green's function. We remark that the charge gap seen in the density of states implies only exponentially small corrections to the entropy of the SK model. Thus the $T=0$ entropy in 0RSB is negative, it becomes much less negative in the improved 1RSB solution below, and (still identical to the one of the SK model) is believed to become zero in the full Parisi solution. The finite part of the entropy at $T=0$ stems from the power-law thermal decay of the order parameter(s), while the charge gap affects the (replica-diagonal) spin autocorrelation and charge correlation, which are related by an operator identity.

B. Improved solutions with broken replica symmetry and strong low-temperature effects

1. Free energy and order parameters

One-step replica symmetry breaking yields a large step towards the exact solution: it allows us to guess properties of it quite frequently. At the beginning of this section, it is useful to rewrite the 1RSB approximation of the free energy in terms of parameters which also allow to obtain finite zero-

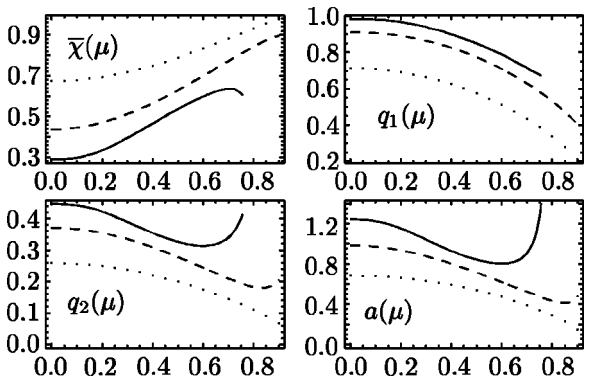

FIG. 5. Order parameters q_1, q_2, nonequilibrium susceptibility $\overline{\chi}$, and normalized Parisi parameter $a \equiv Jm/T$, shown for one-step replica symmetry breaking (1RSB), as a function of the chemical potential μ at selected temperatures $T=0.05J$ (solid lines), $T=0.15J$ (dashed lines), and $T=0.3J$ (dotted lines).

temperature limits. In this way all self-consistent equations, derived from the stationarity condition for the free energy, contain a $T=0$ limit for meaningful finite physical quantities. It is therefore convenient to use the nonequilibrium susceptibility, linear susceptibility, and (temperature-normalized) Parisi parameter denoted, respectively, by $\overline{\chi} = (J/T)(\tilde{q} - q_1)$, $\chi = \overline{\chi} + a(q_1 - q_2)$, and $a = Jm/T$ (we have chosen $\overline{\chi}$, χ, and a as dimensionless).

In these terms the free energy density reads

$$f = \frac{1}{4} J \left[\overline{\chi} \left(\frac{\overline{\chi} T}{J} + 2q_1 - 2 \right) + a(q_1^2 - q_2^2) \right] - T \ln 2 - \mu - \frac{J}{a} \int_{z_2}^{G} \ln \int_{z_1}^{G} \mathcal{C}^{aT/J} \tag{22}$$

with

$$\mathcal{C} = \cosh\left(\frac{J}{T} (\sqrt{q_1 - q_2} z_1 + \sqrt{q_2} z_2) \right) + \cosh\left(\frac{\mu}{T} \right) e^{-(J/2T)\overline{\chi}}. \tag{23}$$

The stationarity condition on f leads to the saddle-point equations for the parameters $\overline{\chi}$, q_1, q_2, and a, which need to be determined as functions of μ and T. The derivation of the thermal self-consistency equations is lengthy. For moderate temperatures, only the numerical solutions are instructive. We present them in Fig. 5 as a function of μ for three characteristic temperatures. In order to facilitate the calculation of the density of states, we have determined the necessary parameters almost continuously on a grid of $(\Delta\mu/J, \Delta T/J) = (10^{-2}, 10^{-2})$.

The above formulation of the free energy allows to obtain the zero-temperature limit in terms of finite quantities

$$f = \frac{1}{2} J \overline{\chi} (q_1 - 1) + \frac{1}{4} J a (q_1^2 - q_2^2) - \mu - \frac{J}{a} \int_{z_2}^{G} \ln \int_{z_1}^{G} \mathcal{C}^{aT/J}. \tag{24}$$

The zero temperature limit of the internal integral is obtained as

$$\begin{aligned} \int_{z_1}^{G} \mathcal{C}^{aT/J} &\to \frac{1}{\sqrt{2\pi}} \int_{-\infty}^{\infty} dz_1 e^{-(z_1^2/2)} e^{a|\sqrt{q_1 - q_2} z_1 + \sqrt{q_2} z_2|} \\ &= \frac{1}{2} e^{a\sqrt{q_2} z_2 + (1/2) a^2 (q_1 - q_2)} \\ &\quad \times \left[1 + \mathrm{erf}\left(\frac{\sqrt{q_2} z_2 + a(q_1 - q_2)}{\sqrt{q_1 - q_2}\sqrt{2}} \right) \right] \\ &\quad + \frac{1}{2} e^{-a\sqrt{q_2} z_2 + (1/2) a^2 (q_1 - q_2)} \\ &\quad \times \left[1 + \mathrm{erf}\left(\frac{-\sqrt{q_2} z_2 + a(q_1 - q_2)}{\sqrt{q_1 - q_2}\sqrt{2}} \right) \right] \end{aligned} \tag{25}$$

for $\mu/J < \overline{\chi}/2$ and

$$\begin{aligned} \int_{z_1}^{G} \mathcal{C}^{aT/J} &= \frac{1}{2} e^{a\sqrt{q_2} z_2 + (1/2) a^2 (q_1 - q_2)} \\ &\quad \times \left[1 + \mathrm{erf}\left(\frac{\sqrt{q_2} z_2 - \left(\frac{\mu}{J} - \frac{\overline{\chi}}{2} \right) + a(q_1 - q_2)}{\sqrt{q_1 - q_2}\sqrt{2}} \right) \right] \\ &\quad + \frac{1}{2} e^{a(\mu/J - \overline{\chi}/2)} \left[\mathrm{erf}\left(\frac{\left(\frac{\mu}{J} - \frac{\overline{\chi}}{2} \right) - \sqrt{q_2} z_2}{\sqrt{q_1 - q_2}\sqrt{2}} \right) \right. \\ &\quad \left. + \mathrm{erf}\left(\frac{\left(\frac{\mu}{J} - \frac{\overline{\chi}}{2} \right) + \sqrt{q_2} z_2}{\sqrt{q_1 - q_2}\sqrt{2}} \right) \right] \\ &\quad + \frac{1}{2} e^{-a\sqrt{q_2} z_2 + (1/2) a^2 (q_1 - q_2)} \\ &\quad \times \left[1 + \mathrm{erf}\left(\frac{-\sqrt{q_2} z_2 - \left(\frac{\mu}{J} - \frac{\overline{\chi}}{2} \right) + a(q_1 - q_2)}{\sqrt{q_1 - q_2}\sqrt{2}} \right) \right] \end{aligned} \tag{26}$$

for $\mu/J > \overline{\chi}/2$.

The preceding $T=0$ results are the basic ingredients which we use analytically to get the self-consistency equations at zero temperature in terms of finite parameters. Results of our final numerical evaluation are collected in Fig. 6.

All of these parameters show a remarkable variation before the first order transition regime to the paramagnetic state is approached at $\mu_{c1}(T=0) \approx 0.881J$. Even q_1, which agrees with the spin autocorrelation function $\tilde{q}$ at $T=0$, contains interesting behavior. This will be extracted below in terms of the change of the fermion filling under one-step replica symmetry breaking.

2. Density of states

The filling factor is an integrated quantity over the density of states folded with the Fermi distribution. We can also exploit the solutions, given so far for the order parameters, in order to determine the fermionic density of states itself.

Using similar techniques as in the RS calculation which led to Eq. (17), the DOS in 1RSB approximation is obtained as

$$\rho(E)=\frac{1}{\sqrt{2\pi}}\sqrt{\frac{1}{TJ\bar{\chi}}}\left[\cosh\left(\frac{\mu}{T}\right)+\cosh\left(\frac{E}{T}\right)\right]e^{-J\bar{\chi}/2T}\int_{z_2}^{G}\frac{\int_{z_1}^{G}\mathcal{C}^{(aT/J)-1}e^{-[-E+(J\sqrt{q_2}z_2+J\sqrt{q_1-q_2}z_1)]^2/(2TJ\bar{\chi})}}{\int_{z_1}^{G}\mathcal{C}^{aT/J}}. \tag{27}$$

In the $T=0$ limit, the saddle-point method allows us to solve the internal integrals exactly, which results in

$$\rho(E)=\frac{1}{\sqrt{2\pi}}\frac{1}{J\sqrt{q_1-q_2}}\begin{cases}0 & \text{for } \mu<J\dfrac{\bar{\chi}}{2} \text{ and } |E|<J\bar{\chi}\\ e^{(a/J)|E|-a\bar{\chi}}\displaystyle\int_{z_2}^{G}\frac{e^{-(1/2)(|E|-J\bar{\chi}-J\sqrt{q_2}z_2)^2/J^2(q_1-q_2)}}{\int_{z_1}^{G}\mathcal{C}^m} & \text{for } \mu<J\dfrac{\bar{\chi}}{2} \text{ and } J\bar{\chi}<|E|\\ e^{a(\mu/J-\bar{\chi}/2)}\displaystyle\int_{z_2}^{G}\frac{e^{-(1/2)(J\sqrt{q_2}z_2-E)^2/J^2(q_1-q_2)}}{\int_{z_1}^{G}\mathcal{C}^m} & \text{for } \mu>J\dfrac{\bar{\chi}}{2} \text{ and } |E|<\mu-\dfrac{J\bar{\chi}}{2}\\ 0 & \text{for } \mu>J\dfrac{\bar{\chi}}{2} \text{ and } \mu-\dfrac{J\bar{\chi}}{2}<|E|<\mu+\dfrac{J\bar{\chi}}{2}\\ e^{(a/J)|E|-a\bar{\chi}}\displaystyle\int_{z_2}^{G}\frac{e^{-(1/2)(|E|-J\bar{\chi}-J\sqrt{q_2}z_2)^2/J^2(q_1-q_2)}}{\int_{z_1}^{G}\mathcal{C}^m} & \text{for } \mu>J\dfrac{\bar{\chi}}{2} \text{ and } \mu+\dfrac{J\bar{\chi}}{2}<|E|\end{cases} \tag{28}$$

where the solutions given by Eqs. (25) and (26) should be substituted.

Figure 7 displays the DOS obtained by exact self-consistent evaluation at one-step replica symmetry breaking. The analytical intermediate solutions described before allowed us to include the $T=0$ solution into the figure (given as bold solid lines). The ensemble of figures shows the band structure at all temperatures below the freezing temperature T_f. The chosen values of μ characterize the evolution of the bands in the range from almost half filling at $\mu=0.05J$ to a filling $\mu=0.7J$ not far from magnetic breakdown $(\sim 0.88J)$.

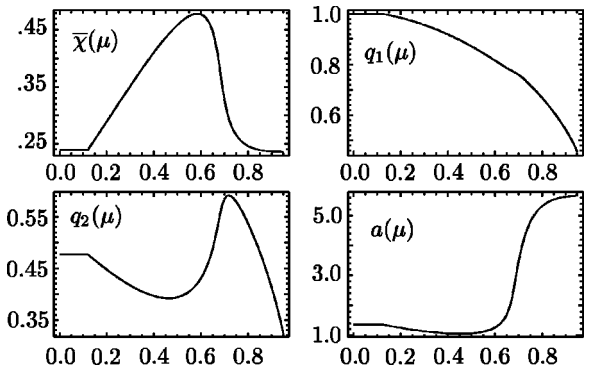

FIG. 6. Order parameters q_1, q_2, nonequilibrium susceptibility $\bar{\chi}$, and normalized Parisi parameter a in 1RSB calculation as a function of the chemical potential (in units of J) at zero temperature.

A comparison with the lowest order approximation, shown in Fig. 2, combined with analytical results for ∞RSB, gives a clear hint at the exact ISG$_f$ solution. Only the first part for $\mu=0.05J<\frac{1}{2}E_g^{(1)}\approx 0.119J$ does not contain the central band, since $\nu(\mu=0.05J, T=0)=1$ in 1RSB. For $E_g^{(1)}=0.119J<\mu<E_g^{(0)}=\sqrt{2/\pi}J$ the central band is present in 1RSB, while it was absent in RS in this interval. This effect sets in at low temperatures, corresponding to the smaller magnetic energy scales set by the new additional order parameter of 1RSB.

Also in this approximation, the appearance of the central peak in the spectral weight is linked to a random field crossover line, determined by $\partial^2 f/\partial\tilde{q}^2=0$ (see Fig. 1). At $\mu=0.5J$, the central band is already well developed for low enough temperatures. Here, the lowest order approximation leads only to a very small band, since $\mu=0.5J$ exceeds only by little the RS gap edge.

As for half filling the ratio between the gap widths and the (finite) DOS at the gap edge is constant. For higher order symmetry breaking the gap shrinks and the spectral weight at the edge diminishes correspondingly; thus spectral weight is moved into parts of the gap region, as the approximation is improved step by step.

The crossover from finite low T to the exact $T=0$ solutions, shown by fat lines in the three-dimensional (3D) plots, redistributes considerably the spectral weight. At higher μ, for example $\mu=0.7J$ as shown in Fig. 7, the central band shows a maximum also as a function of temperature. The DOS height in the center decreases again at lowest temperatures, the band becomes broader at $T=0$.

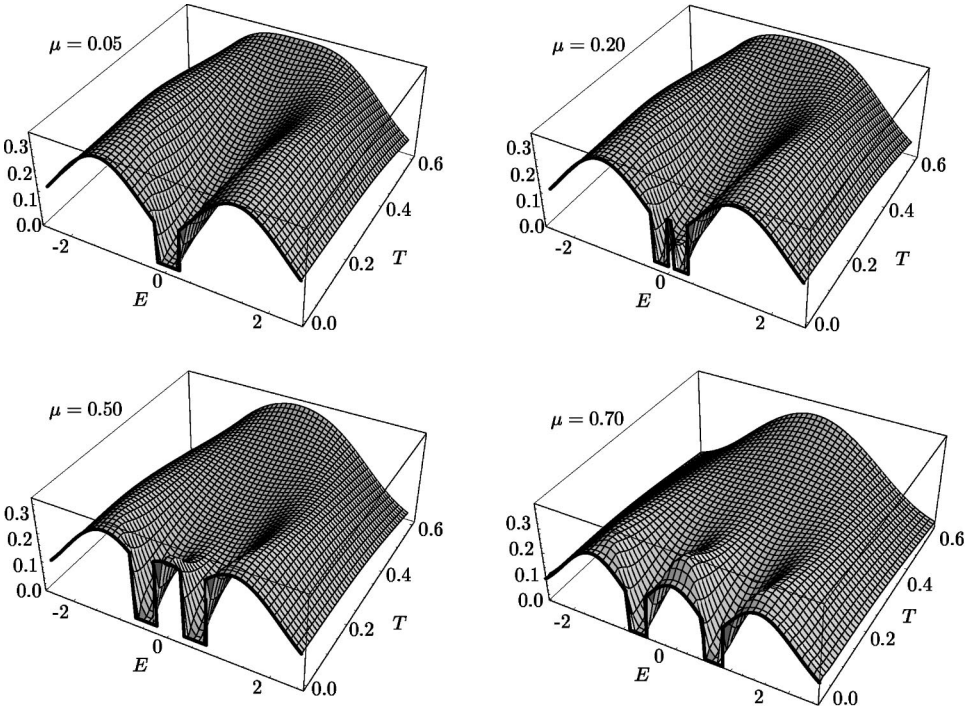

FIG. 7. Density of states at finite and at zero temperature in 1RSB shown for $\mu/J=0.05$, 0.2, 0.5, and 0.7 as a function of energy $E=\epsilon+\mu$ and temperature T (μ, E, and T displayed in units of J).

Comparing the $T=0$ limit of Figs. 2 and 4, which show the RS approximation, with that of Fig. 7 for the first improved 1RSB approximation, one finds that replica symmetry breaking leads to a refinement of the band structure. Each further RSB step, until the exact ∞RSB solution is reached, will modify magnetic and nonmagnetic bands according to the still smaller scales and magnetic order parameters. However, although one step RSB does not yet yield the exact solution of this model, further refinements are much smaller in size and it is possible to imagine the exact result from our Fig. 7. For zero temperature, as a function of a continuously varying chemical potential, the 1RSB solution for the density of states is displayed in Fig. 8. The tendency of RSB effects is obvious by comparison with Fig. 4.

The central band maintains the wedgelike shape already observed in the replica symmetric result. Its thick end however shows a new structure near the discontinuous magnetic breakdown, while the other end progressed by a large step towards $\mu=0$. The distance from $\mu=0$ will be further reduced in kRSB with $k>1$ and vanishes for $k\to\infty$.

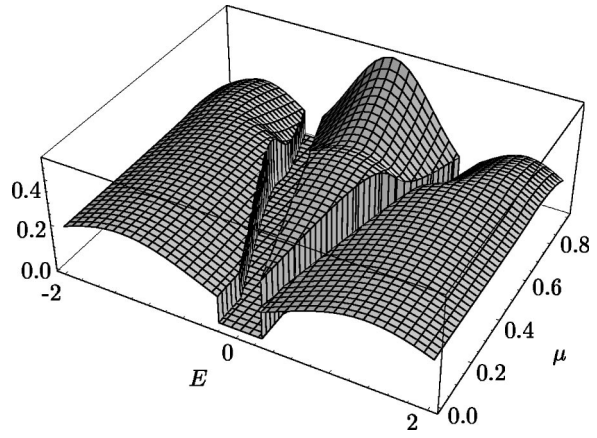

FIG. 8. DOS at $T=0$ for 1RSB. The central band appears above $\mu\approx 0.119J$ (DOS, E, and μ shown in units of J).

3. Infinite breaking of replica symmetry

The top of the wedge reaches $\mu=0$ in ∞RSB and at the same time the gap widths approach zero; the DOS still vanishes at $\pm\mu$ but stays finite yet very small in the vicinity of $E=\pm\mu$. The derivation of this feature is analogous to the one presented in Ref. 8: The ratio between gap width and DOS size at the gap edge is invariant under RSB and hence both quantities decay together to zero in the limit of infinite RSB. Here it is assumed that the nonequilibrium susceptibility, which determines the gap width at any order k of the RSB, approaches zero for $k\to\infty$ as in the half filled case. The latter result was inferred from the work of Thouless, Anderson, and Palmer.[10]

IV. CONNECTION BETWEEN FERMION CONCENTRATION AND REPLICA SYMMETRY BREAKING

The filling factor can be described by the summation over the imaginary frequency Green's function $\mathcal{G}$ by

$$\nu=T\sum_{\epsilon_n,\sigma}\mathcal{G}_\sigma(\epsilon_n)e^{i\epsilon 0_+}. \tag{29}$$

The Green's function is related to the density of states discussed before by the usual spectral representation $\mathcal{G}(\epsilon_l)=\int d\epsilon[\rho(\epsilon)/i\epsilon_l-\epsilon]$ [and by $\rho(\epsilon)=-(1/\pi)\mathrm{Im}(G^R(\epsilon))$], which means that the whole fermion propagator changes under RSB. Still the summation over all frequencies could either wipe out or maintain this dependence. Indeed, what we find is a transition between these two alternatives inside the ordered phase.

We have emphasized the role of replica symmetry breaking for quantum dynamics and low-energy excitations. Despite the absence of quantum dynamics in charge correlations, and despite the absence of spin-charge couplings in the

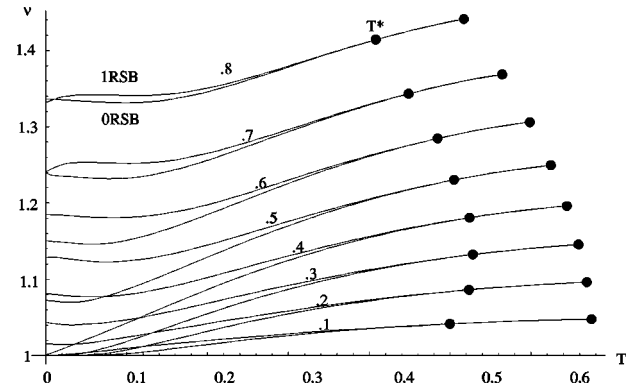

FIG. 9. Results for the temperature dependence of the filling factors in RS and 1RSB are grouped together for $0.1 \leqslant \mu/J \leqslant 0.8$ with $\Delta\mu/J=0.1$ ($T,\Delta\mu$ given in units of J). The right endpoints of all pairs of lines denote the freezing temperatures $T_f(\mu)$, while at the intermediate points T^*, displayed for the pair at $\mu=0.8J$, the fillings ν_{RS} and ν_{1RSB} differ by only $O(10^{-4})$. Zeros of $\nu_{RS}-\nu_{1RSB}$ exist within $T^*(\mu)<T<T_f(\mu)$ and at low T for $\mu>0.7J$.

Hamiltonian, we find that replica symmetry breaking affects spin-correlations and charge-average in a qualitatively different way.

In one-step breaking we report in this section a crossover line, which separates a regime of almost invisible RSB effects in the filling factor and in $\tilde{q}$ from one with large RSB effects in these quantities. The magnetic order parameter does not show any sign of this crossover. The announcement of these effects evokes on one hand the old, resolved problem[16] of absence of RSB below the freezing temperature, and on the other hand the phenomenon of a Gabay-Toulouse line,[17] followed by a crossover to a region with RSB effects in all order parameters.[18]

The first case bears no relation with our case: the present model is static in charge and spin correlation and the particular role of dynamic effects,[16] which occurred in the transverse field Ising model, do not exist here. The crossover line describing the onset of RSB in transversal correlations of a Heisenberg spin glass in a magnetic field, however, has a vague resemblance, provided we imagine charge degrees of freedom as transversal with respect to spin. The chemical potential then roughly corresponds to the magnetic field in the standard case. However, a detailed mapping between the two models does not seem feasible.

In Fig. 9 the fermion filling factor is shown. Pairs of $[\nu_{RS(\mu)},\nu_{1RSB}(\mu)]$ are grouped together for $\mu/J=0.1,0.2,\ldots,0.8$. The detailed plots contain two interesting features: each pair of lines seems to merge asymptotically, but the lines still cross each other at a $T_0^*(\mu)$, staying close together for $T_0^*(\mu)<T<T_f(\mu)$. Since the lines cross, having almost identical slope, it is difficult to determine with sufficient numerical precision the line $T_0^*(\mu)$ of crossings. We therefore chose points $T^*(\mu)$ where RS and 1RSB lines differ only by 10^{-4}. In between these points and the end points at the freezing temperature corresponding to the μ parameter of each curve, the RS and 1RSB curves cross at least once.

The interesting fact now is that there is a region below the freezing temperature, where replica symmetry breaking effects in the fermion filling factor almost vanish. While this occurs in the charge related quantity, the magnetic observables such as order parameters show large RSB effects. One may find it surprising that RSB effects appear at all in the fermion concentration.

In addition to the separation of magnetic and nonmagnetic bands described before for the ordered phase, one also finds a different exposure of charge- and spin-related quantities to the effects of replica symmetry breaking. None of the quantities is excluded from this, despite the fact that the model does not contain a spin-charge interaction. The only coupling is mediated by the chemical potential.

At zero temperature, this crossover is most pronounced. Beyond the crossing point of the two approximations at $\mu^* \approx 0.7J$ both lines stay close together as if no symmetry-breaking effect would occur at all between μ^* and the discontinuous breakdown of magnetic order at $\mu_1 \approx 0.881J$. On the other side, for $\mu<\mu^*$ the RSB effect is large. Moreover, the right-hand side of Fig. 10 shows for comparison the numerical result for the corresponding TAP equation of finite-size systems.[19] This generalized TAP result should correspond to the full Parisi solution with ∞RSB. At $T=0$ the filling ν starts to differ from one, when the chemical potential moves through the gap edge. The gap size depends on the number of RSB steps and decreases to zero in the ∞RSB solution. Thus it is clear that the left end point of the filling curve $\nu(\mu)$ moves into $(\nu=1,\mu=0)$. The change from the

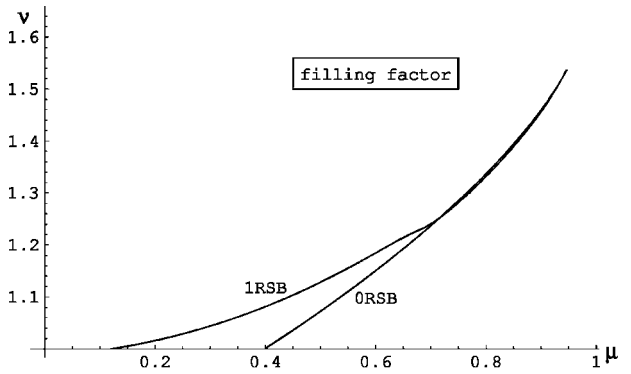

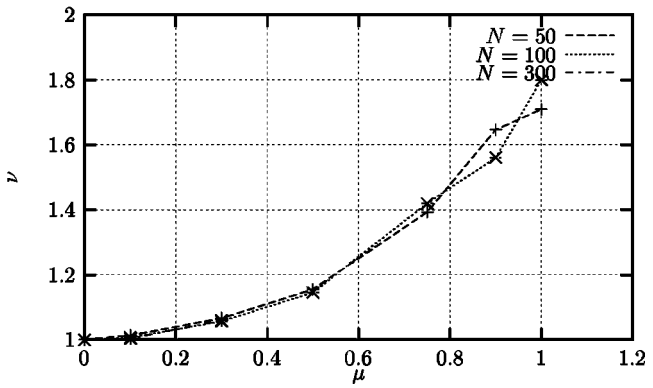

FIG. 10. The filling factor at $T=0$, shown as a function of the chemical potential μ (T,μ in units of J). The RS and 1RSB results of this paper are included in the figure on the left-hand side, while on the right the numerical solution of the corresponding TAP equations is taken from Ref. 18 for comparison. There, N denotes the system size.

calculated one-step RSB solution to this exact one is much smaller than the one from RS to 1RSB. The shape of the 1RSB solution resembles almost perfectly the one found numerically from the generalized TAP equation. Also quantitative agreement is obtained for $\mu < 0.5J$. The nonvanishing kRSB corrections for $k=2$ and higher can be expected to be almost invisibly small. Deviations in the high-μ region might be due to numerical problems of the algorithm in Ref. 19 either because of the vicinity of the first order phase transition or due to finite-size effects.

In general, however, the TAP solution is already in good agreement with the analytical 1RSB solution, whose extension to the full RSB solution is obvious. The flat increase of the integrated quantity $\nu(\mu)$ from 1 (probably with slope zero) in the generalized Parisi solution is consistent with the fact that for rare nonmagnetic regions the central band does not start as a δ peak, but as function with finite height and a width increasing smoothly from zero as μ becomes finite.

V. SUMMARY AND OUTLOOK

We presented a complete analysis of the band structure of the fermionic Ising spin glass for arbitrary doping. The numerical study for finite temperatures was accompanied by analytical results for $T=0$, all evaluated up to first step replica symmetry breaking. A three-band structure formed by two magnetic side bands and a central nonmagnetic band was obtained in the ordered phase. The nonmagnetic central band shows rapid growth as the temperature decreases, but also nonmonotonic behavior. Its becomes particularly pronounced in the low-temperature regime below a crossover line defined by $\partial^2 f/\partial \tilde{q}^2 = 0$. While a random-field-like instability is prevented by the off-diagonal order parameters $q^{a\neq b}$, the sign change of this second derivative of the free energy implies a strong increase of the deviation from half filling, which is of course related to the central band.

At $T=0$ we found a complete separation of the bands, the separation being finite in any approximation using a finite number of RSB steps and finally zero in the exact solution. This was concluded by means of an exact relation for infinite-step symmetry breaking.

We thus demonstrated strong RSB effects on the magnetic order parameters, on the density of states (DOS), on quantum dynamics included in the fermion Green's function, and even on the integrated DOS, which equals the fermion concentration at $T=0$ (seen as a function of chemical potential).

It is interesting to compare the evolution of central nonmagnetic bands in disorder-free Hubbard and Kondo lattice models[3] with the one of the present random interaction model: the role of spin glass order as the source for band gaps and the Parisi symmetry forming their shape-giving mechanism can then be particularly appreciated.

Our present results for the nonitinerant spin glass also imply important questions and suggestions on itinerant extensions. If one speculates that a pseudogap is filled by coupling to a conduction band, for example, the question of Anderson localized states around the Fermi level must be raised. The more fundamental questions will, however, be whether replica symmetry breaking survives in the presence of transport. In Hubbard models the hopping expansion around the atomic limit is singular, but this does not seem to be the case in the itinerant spin glass. If so, the possibility of localization in the pseudogap regime of small DOS will not only be decisive for ac and dc conductivity but will also carry signs of replica symmetry breaking.

Since exact mean-field solutions of metallic spin glass models are at least as hard to find as the $d=\infty$ solution of the Hubbard model, meaningful approximate solutions are welcome in both cases. In particular, a comparison with the fully frustrated Hubbard model in infinite dimensions[20] would be of high interest.

ACKNOWLEDGMENTS

We are indebted to M. Kiselev, E. Nakhmedov, and D. Sherrington for discussions. This work was supported by the Deutsche Forschungsgemeinschaft under Contract No. Op28/5-1 and by the SFB410. Further support by the Villigst foundation (H.F.) and by the EPSRC (R.O.) is gratefully acknowledged.

[1] A. Georges, G. Kotliar, W. Krauth, and M. Rozenberg, Rev. Mod. Phys. **68**, 13 (1996).
[2] A. Auerbach, in *Correlated Electron Systems*, edited by V. J. Emery (World Scientific, Singapore, 1992).
[3] P. Nozières, Eur. Phys. J. B **6**, 447 (1998).
[4] G. Parisi, J. Phys. A **13**, 1887 (1980).
[5] G. Parisi, J. Phys. A **13**, L115 (1980).
[6] K. Binder and A. Young, Rev. Mod. Phys. **58**, 801 (1986).
[7] K. H. Fischer and J. Hertz, *Spin Glasses* (Cambridge University Press, Cambridge, 1991).
[8] R. Oppermann and B. Rosenow, Europhys. Lett. **41**, 525 (1998).
[9] F. A. da Costa, C. S. O. Yokoi, and S. R. A. Salinas, J. Phys. A **27**, 3365 (1994).
[10] D. Thouless, P. Anderson, and R. Palmer, Philos. Mag. **35**, 593 (1977).
[11] B. Rosenow and R. Oppermann, Phys. Rev. Lett. **77**, 1608 (1996).
[12] H. Feldmann and R. Oppermann, Eur. Phys. J. B **10**, 429 (1999).
[13] H. Feldmann and R. Oppermann, J. Phys. A (to be published).
[14] R. Oppermann and A. Müller-Groeling, Nucl. Phys. B **401**, 507 (1993).
[15] R. Oppermann and B. Rosenow, Phys. Rev. B **60**, 10 325 (1999).
[16] G. Büttner and K. D. Usadel, Phys. Rev. B **41**, 428 (1990).
[17] M. Gabay and G. Toulouse, Phys. Rev. Lett. **47**, 201 (1981).
[18] D. M. Cragg, D. Sherrington, and M. Gabay, Phys. Rev. Lett. **49**, 158 (1982).
[19] M. Rehker and R. Oppermann, J. Phys.: Condens. Matter **11**, 1537 (1999).
[20] G. Kotliar, cond-mat/9903188 (unpublished).